Modeling surfzone tracer plumes, Part 2: Transport and dispersion

David B. Clark

Falk Feddersen

R. T. Guza

Scripps Institution of Oceanography, La Jolla, California

Abstract. Five surfzone dye tracer releases from the HB06 experiment are simulated with a tracer advection diffusion model coupled to a Boussinesq surfzone model (`funwaveC`). Model tracer is transported and stirred by currents and eddies, and diffused with a breaking wave eddy diffusivity, set equal to the breaking wave eddy viscosity, and a small (0.01 $\mathrm{m^2\,s^{-1}}$) background diffusivity. Observed and modeled alongshore parallel tracer plumes, transported by the wave driven alongshore current, have qualitatively similar cross-shore structures. Although the model skill for mean tracer concentration is variable (from negative to 0.73) depending upon release, cross-shore integrated tracer moments (normalized by the cross-shore tracer integral) have consistently high skills (≈ 0.9). Modeled and observed bulk surfzone cross-shore diffusivity estimates are also similar, with 0.72 squared correlation and skill of 0.4. Similar to the observations, the model bulk (absolute) cross-shore diffusivity is consistent with a mixing-length parameterization based on low frequency (0.001–0.03 Hz) eddies. The model absolute cross-shore dispersion is dominated by stirring from surfzone eddies, and does not depend upon the presence of the breaking wave eddy diffusivity. Given only the bathymetry and incident wave field, the coupled Boussinesq-tracer model qualitatively reproduces the observed cross-shore absolute tracer dispersion, suggesting that the model can be used to study surfzone tracer dispersion mechanisms.

1. Introduction

The rates and mechanisms of surfzone horizontal tracer (e.g., pollution, nutrients, sediment, and larvae) dispersion are understood poorly, and numerical models may be useful for investigating the underlying dispersion processes. However, numerical surfzone tracer models have not been validated, a necessary step before investigating dispersion mechanisms.

Surfzone tracer dispersion has been modeled analytically and numerically. Simple Fickian analytic models were used to estimate bulk surfzone diffusivity from field data [*Harris et al.*, 1963; *Inman et al.*, 1971; *Clarke et al.*, 2007; *Clark et al.*, 2010]. Fickian models may be able to predict bulk surfzone tracer dispersion with the appropriate diffusion coefficient. However, surfzone diffusivity values are poorly known, and diffusivity parameterizations have not been validated over a broad range of conditions. Coupled tracer and (wave-averaged) circulation models have been sparingly used to simulate tracer transport in the nearshore and surfzone [*Tao and JianHua*, 2006; *Issa et al.*, 2010], but comparisons with observations are very limited [*Rodriguez et al.*, 1995].

Scaling arguments [*Harris et al.*, 1963; *Inman et al.*, 1971] and an idealized model [*Feddersen*, 2007; *Henderson*, 2007] suggest that the bulk (averaged over many waves) cross-shore tracer diffusivity κ_{xx} from turbulent-mixing at the front face of broken waves (bores) scales as $\kappa_{xx} \propto H_{\rm s}^2 T_{\rm m}^{-1}$, where $H_{\rm s}$ and $T_{\rm m}$ are the incident significant wave height and mean period, respectively. However, this scaling had marginal correlation ($r^2 = 0.32$) when compared with recently observed bulk cross-shore dye diffusivities [*Clark et al.*, 2010]. Stirring due to low frequency ($f < 0.03$ Hz) horizontal surfzone eddies may induce a significant amount of cross-shore tracer dispersion. Higher correlation ($r^2 = 0.59$) was found for a surfzone-eddy

mixing-length scaling $\kappa_{xx} \propto \overline{V}_{\rm rot}^{\rm (IG)} L_x$, where L_x is the surfzone width and $\overline{V}_{\rm rot}^{\rm (IG)}$ is a surfzone (cross-shore) averaged bulk infragravity (0.004–0.03 Hz) eddy velocity, suggesting that low-frequency eddies may be a primary dispersion mechanism [*Clark et al.*, 2010]. An undertow-induced cross-shore shear dispersion scaling [*Pearson et al.*, 2009] was not found to be applicable [*Clark et al.*, 2010]. Overall, the mechanisms of tracer dispersion and their relative importance are not well understood.

Time-dependent wave-resolving surfzone models (most commonly Boussinesq models), include the broad range of processes, from individual breaking waves to low frequency eddies and mean currents, required for investigating surfzone tracer dispersion mechanisms. Boussinesq surfzone models, solving an extended version of the nonlinear shallow water equations with weak nonlinearity and dispersion [e.g., *Peregrine*, 1967; *Nwogu*, 1993; *Wei et al.*, 1995, and many others], have been used to examine surfzone drifter dispersion in directionally-spread random wave fields [*Johnson and Pattiaratchi*, 2006; *Spydell and Feddersen*, 2009; *Geiman et al.*, 2011], but have not been used for surfzone tracer modeling. Finite-crest-length wave breaking within Boussinesq models provide a (vertical) vorticity source for forcing horizontal eddies [*Peregrine*, 1998] at a range of length-scales, which induced surfzone drifter dispersion at scales between 20–200 m [*Spydell and Feddersen*, 2009]. Surfzone drifters duck under, and are not dispersed by entrainment in, the front face of breaking waves [e.g., *Schmidt et al.*, 2003, 2005]. By resolving individual wave breaking, Boussinesq models also providing a mechanisms for breaking waves to mix tracer. Thus, a depth-averaged tracer advection diffusion equation coupled to a Boussinesq model contains both stirring by the horizontal eddy field (e.g., vertical vorticity) and the breaking wave mixing mechanisms.

Here, five surfzone tracer releases from the HB06 experiment in Huntington Beach, California [*Clark et al.*, 2010] are simulated with the coupled tracer and Boussinesq model `funwaveC`. The Boussinesq model is described in *Feddersen et al.* [2011], hereafter [Part-1], and compared with Eulerian wave and current observations. The model reproduces the observed significant wave height and (except for one release) alongshore currents. Low frequency eddies are well modeled in the infragravity frequency (f) band ($0.004 < f < 0.03$ Hz), but are overpredicted by a factor of 2 in the very low frequency (VLF, $0.001 < f < 0.004$ Hz) band. The HB06 tracer experiments and previous results are summarized in Section 2. The tracer model and averaging method are described in Section 3.

Mean tracer concentrations are well modeled for 3 out of 5 releases (Section 4). For all releases, model skills for cross-shore integrated tracer first and second moments are high, and the model reproduces the observed bulk cross-shore surfzone diffusivity (Section 5). The causes of model-data mismatch for mean tracer and alongshore tracer transport are discussed in Sections 6.1 and 6.2, respectively. The downstream dilution of the modeled mean plume is consistent with a Fickian analytic solution (Section 6.3). The effect of the modeled breaking wave eddy diffusivity on cross-shore tracer dispersion is discussed in Section 6.4. Mixing-length scalings for modeled bulk cross-shore diffusivity κ_{xx}, using bulk low frequency eddy velocities, are examined in Section 6.5. The results are summarized in Section 7.

2. HB06 observations and dye releases

The predominant south swell during the HB06 experiment drove strong alongshore currents upcoast (towards the northwest). Waves and currents were measured on a 140 m long cross-shore array of 7 bottom mounted tripods, denoted F1-F7 from near the shoreline to roughly 4 m water depth [Figure 1, Part-1]. The observations at F2 were often poor quality, and are

not included in the subsequent analysis. Hourly significant wave heights $H_{\rm s}$ ranged from 0.41–1.02 m during the tracer releases, with mean wave periods $T_{\rm m}$ from 9–9.9 s, and directional spreads σ_θ from 15–23 degrees. Mean (in time) alongshore currents $V(x)$ (where x is the cross-shore distance from the shoreline) were generally maximum near mid-surfzone, except for one release with maximum $V(x)$ near the shoreline. Eulerian wave and current observations are described in *Clark et al.* [2010] and compared with the `funwaveC`Boussinesq model in [Part-1].

Five continuous dye tracer releases (denoted R1, R2, R3, R4, and R6) were performed on different days [*Clark et al.*, 2010]. Dye tracer was injected 0.5 m above the bed in roughly 1 m water depth (4–54 m from the shoreline), at rates between $1.3-7.1\ {\rm mL\,s^{-1}}$(263–$1489\ {\rm ppb\,m^3\,s^{-1}}$). The tracer was advected downstream with the mean alongshore current, forming shore parallel plumes, and measured near the surface for between 40–121 minutes (depending on the release) with a jet ski mounted fluorometer system [*Clark et al.*, 2009].

Visual observation indicated rapid vertical tracer mixing (tracer reaching the surface within several meters of the source), and patchy and highly variable tracer plumes. Dye was sampled on repeated cross-shore transects at 3–9 downstream locations, between 16–565 m from the tracer source. With increasing downstream distance y from the dye source, the mean cross-shore tracer profile $D(x,y)$ peak concentrations decreased and cross-shore widths increased. The cross-shore profiles were often shoreline attached, roughly resembling a half-Gaussian, with a maxima near the shoreline. Bulk cross-shore surfzone diffusivities κ_{xx} were estimated from the downstream evolution of the plume squared cross-shore length scale, and varied between 0.5–2.5 ${\rm m^2\,s^{-1}}$[*Clark et al.*, 2010].

3. Surfzone tracer modeling and analysis

3.1. Tracer model description

The 5 tracer releases analyzed in *Clark et al.* [2010] are simulated with a time-dependent wave-resolving Boussinesq model (`funwaveC`, [Part-1]). The model bathymetry is based on the observed alongshore-averaged survey bathymetry (Figure 1b). Waves matching the observed incident angle, directional spread, and energy spectrum are generated by the model wavemaker, and propagate towards the shore where they "break" and dissipate (by the breaking eddy viscosity $\nu_{\rm br}$). Model wave breaking drives alongshore currents and low-frequency ($f < 0.03$ Hz) surfzone eddies. The observed significant wave height $H_{\rm s}(x)$, mean alongshore current $V(x)$, and bulk rotational infragravity (IG) velocities $\mathcal{V}_{\rm rot}^{\rm (IG)}(x)$ are modeled with high skill. Bulk very-low-frequency (VLF) rotational velocities were overpredicted by about a factor of 2 [Part 1].

A depth-averaged tracer module, coupled to the time-dependent Boussinesq model `funwaveC`, allows for three separate non-interacting tracers (denoted A, B, and C) released at different locations. Each tracer samples a different part of the flow field, increasing the degrees of freedom for quantities averaged over the statistics of all three tracers. Model tracer evolves according to an advection-diffusion equation,

$$\frac{\partial[(h+\eta)d]}{\partial t} + \boldsymbol{\nabla}\cdot[(h+\eta)\boldsymbol{u}d] = \boldsymbol{\nabla}\cdot[(\kappa_{\rm br}+\kappa_0)(h+\eta)\boldsymbol{\nabla}d] + M_0\delta(x-x_{\rm rl})\delta(Y-Y_{\rm rl}) \quad (1)$$

where d is the tracer concentration (in ppb), h is the still water depth, η is the free surface elevation, $\kappa_{\rm br}$ is the breaking-wave eddy diffusivity, κ_0 is the background diffusivity, $\boldsymbol{\nabla}$ is the two-dimensional horizontal gradient operator, and $\boldsymbol{u}$ is the model horizontal velocity vector, which for small kh is approximately the depth-averaged velocity. Tracer is injected into the model at $(x = x_{\rm rl}, Y = Y_{\rm rl})$ with the input flux M_0 (δ is the Kronecker delta function).

In (1), $\kappa_{\rm br}$ is set equal to the the breaking-wave eddy viscosity $\nu_{\rm br}$ (e.g., momentum and tracer are assumed to mix identically), and the background diffusivity $\kappa_0 = 0.01\ {\rm m^2\,s^{-1}}$, is two orders of magnitude smaller than the observed bulk κ_{xx}. The $\kappa_{\rm br}$ is non-zero only on the front face of a breaking-wave (bore), whereas κ_0 is applied everywhere. The inclusion of the breaking eddy viscosity allows the breaking-wave mixing mechanism discussed in *Feddersen* [2007] to be examined relative to other tracer dispersion mechanisms.

The vertically-integrated Boussinesq and tracer models lack cross-shore dispersion by vertically sheared currents (i.e., undertow). However, this mechanism was not found to be significant in a natural surfzone with directionally spread waves [*Clark et al.*, 2010], and rapid vertical mixing [*Feddersen and Trowbridge*, 2005; *Ruessink*, 2010; *Feddersen*, 2011] implies little vertical tracer structure within the surfzone. However, vertical structure may be important seaward of the surfzone [*Kim and Lynett*, 2010].

The cross-shore tracer domain (dashed lines, Figure 1a) is embedded in the full Boussinesq model domain. The offshore tracer boundary (set to $D = 0$ ppb) is located just onshore of the wavemaker region between $x = 232 - 260$ m from the shoreline, depending upon release. The onshore tracer boundary is typically located ≈ 5 m onshore of the start of the sponge layer (the depth of the flat region is $h_0 = 0.2 - 0.35$ m), where a no-flux boundary condition is applied. In contrast to the η and $\boldsymbol{u}$ periodic alongshore boundary conditions, the tracer alongshore boundary conditions (at both ends of the 1500 m alongshore domain) are open, allowing tracer to advect out of the domain (Figure 1a). The alongshore tracer boundary conditions affect tracer concentrations within approximately 25 m of the boundary, and these regions are excluded from the analysis.

The model spins up for 2000 s before starting continuous releases of tracers A, B, and C at alongshore locations $Y_{\rm rl} = 250$, 500, and 750 m, respectively, from the upstream boundary (Figure 1a). Model and observed cross-shore release locations $x_{\rm rl}$ and tracer injection rates M_0 are equal (Table 1). Model instantaneous tracer concentrations $d^{(\rm A,B,C)}$, sea surface elevation η, cross- and alongshore currents (u and v), and breaking wave eddy diffusivity $\kappa_{\rm br}$ are output every 2 seconds over the entire domain.

3.2. Model tracer analysis: averaging

The model tracer advects downstream with the mean alongshore current forming a shore-parallel plume that widens with downstream distance. Instantaneous $d^{(\rm A)}$ model tracer plumes (Figure 2a,c,e) are variable and patchy, with eddy-like tracer structure seaward of the surfzone ($x < -100$ m). The cross-shore structure of modeled low frequency rotational motions (i.e., eddies) is discussed in [Part-1].

The $D^{(\rm A)}(x,y)$, $D^{(\rm B)}(x,y)$, and $D^{(\rm C)}(x,y)$ represent mean modeled tracers A, B, and C, time-averaged in a fixed reference frame ($x = 0$ m at the shoreline and $y = 0$ m at the release location) between 6000–14,000 s after the tracer release started. Time-averaging begins once the tracer plume has reached quasi-equilibrium (see Figure 3). The averaging times used for the observed means $D^{(\rm obs)}$ are limited by instrument and environmental parameters to between 40-120 min. The model averages are over 133 min (8000 s) after tracer is equilibrated (Figure 3). Stability of the numerical results is further increased by averaging statistics over tracers A, B, and C. Averages over one 5600 s wavemaker recurrence cycle [Part-1] are nearly identical to the 8000 s averages presented here, suggesting the wavemaker recurrence does not effect the tracer results significantly. The observed $D^{(\rm obs)}$ (this notation differs slightly from *Clark et al.* [2010]) and model $D^{(\rm A,B,C)}$ mean plumes are time-averaged in fixed coordinates (i.e., absolute aver-

aged), which includes any plume meandering in the resulting (absolute) diffusivity estimates. Relative averaging [e.g., in center of mass coordinates, *Csanady*, 1973], which separates plume meandering from smaller scale mixing, is not used here because the interpretation of relative averages is unclear near the shoreline boundary [*Clark et al.*, 2010].

Mean tracer $D^{(\mathrm{A})}$ plumes (Figure 2b,d,f) are much smoother than the instantaneous tracer (Figure 2a,c,e). The absolute concentration (in ppb) varies between model releases (relative shades of gray between panels in Figure 2), due to different tracer injection rates (Table 1), different V magnitudes (stronger V decreases tracer concentrations for a given injection rate), and varying amount of cross-shore dispersion.

4. Mean cross-shore tracer profiles and alongshore tracer transport

4.1. Mean cross-shore tracer profiles

Model $D^{(\mathrm{A})}$ and observed $D^{(\mathrm{obs})}$ mean tracer profiles at three representative downstream y are shown for all releases in Figure 4. $D^{(\mathrm{A})}$ and $D^{(\mathrm{obs})}$ profiles for R3, R4, and R6 are usually shoreline attached (maxima at or near the shoreline), with decreasing peak concentrations and increasing cross-shore widths with downstream distance y (Figure 4c,d,e). The mean tracer concentration skill for each transect is estimated by $1 - \langle (D^{(\mathrm{obs})}(x,y) - D^{(\mathrm{A,B,C})}(x,y))^2 \rangle_{x,y} / \langle D^{2\,(\mathrm{obs})}(x,y) \rangle_{x,y}$, where $\langle\rangle_{x,y}$ is the mean over x and y, for regions where $D^{(\mathrm{obs})} > 5$ ppb (thus avoiding relatively large instrument noise at low concentrations). Mean R3, R4 and R6 skills, averaged over all transects and the three model tracers in each release, are between 0.5 and 0.73 (Table 2), consistent with the qualitative agreement in Figure 4c,d,e.

For release R1, the magnitudes and shapes of $D^{(\mathrm{A})}$ and $D^{(\mathrm{obs})}$ are roughly similar, and both model and observed mean tracer spread in the cross-shore with downstream distance (Figure 4a). However, at $y = 56$ and 107 m the $D^{(\mathrm{obs})}$ maximum is farther to the shoreline than

for $D^{(\mathrm{A})}$ (Figure 4a), which may be explained by seaward advection of the observed plume [*Clark et al.*, 2010]. This cross-shore displacement between $D^{(\mathrm{A})}$ and $D^{(\mathrm{obs})}$ maxima results in negative skill for R1 (Table 2), despite the similarity in shape.

The R2 $D^{(\mathrm{A})}$ disperses similarly to $D^{(\mathrm{obs})}$, however the $D^{(\mathrm{A})}$ magnitudes are significantly larger than $D^{(\mathrm{obs})}$ (Figure 4b) which results in negative skill (Table 2). The differences in mean tracer magnitude are most pronounced near the shoreline where $D^{(\mathrm{A})}$ are often 2–5 times larger than $D^{(\mathrm{obs})}$ (Figure 4b).

4.2. Alongshore tracer transport

Model $M^{(\mathrm{A,B,C})}(y)$ and observed $M^{(\mathrm{obs})}(y)$ alongshore tracer transports are [*Clark et al.*, 2010]

$$M(y) = \int_{x_{\mathrm{F7}}}^{x_{\mathrm{in}}} h(x)V(x,y)D(x,y)\,dx, \tag{2}$$

where x_{in} is the observed inner transect edge (i.e., where observations end near the shoreline, Figure 4), x_{F7} is the F7 location (the farthest seaward velocity observation), and $V(x,y)$ is the mean alongshore current averaged over the same times as $D(x,y)$. Note that the model $M^{(\mathrm{A,B,C})}$ uses alongshore varying $V(x,y)$ while the observations assume alongshore uniform $V(x)$ as measured on the cross-shore array. The model $V(x,y)$ vary weakly alongshore [Part-1], and using alongshore averaged model $V(x)$ does not change $M^{(\mathrm{A,B,C})}$ significantly. The x_{in} range from -17 to -10 m, and x_{F7} range from -146 to -162 m from the shoreline. This $M(y)$ estimate excludes the region shoreward of x_{in} and seaward of x_{F7}, and excludes alongshore eddy tracer fluxes by using time averaged V and D.

The $M^{(\mathrm{A,B,C})}$ and $M^{(\mathrm{obs})}$ have roughly similar structure and decrease slightly at large y, except the overestimated $M^{(\mathrm{A,B,C})}$ in R3 (Figure 5). Estimates between individual $M^{(\mathrm{A})}$, $M^{(\mathrm{B})}$, and $M^{(\mathrm{C})}$, sometimes vary by 50%. The model tracer input flux is equal to the observed dye re-

lease flux $M^{(\mathrm{obs})}(y=0)$ (circles in Figure 5), however the $M^{(\mathrm{A,B,C})}$ do not necessarily match at the source and are not conserved downstream. The difference between the observed input flux ($y=0$, circles in Figure 5) and observed and modeled downstream transport $M^{(\mathrm{obs})}(y>0)$ may be due to neglected alongshore eddy fluxes in (2) or to tracer transported onshore of x_{in} (e.g., R3 $D^{(\mathrm{A})}$ at $x>-15$ m in Figure 4c) or offshore of x_{F7}. For the model, this is examined in Section 6.2.

5. Cross-shore integrated tracer moments and bulk surfzone diffusivity κ_{xx}

5.1. Definitions

Observed and modeled cross-shore tracer plume structures are compared using cross-shore integrated surface tracer moments, which are consistent with a Fickian framework [*Clark et al.*, 2010]. These moments are normalized by the total tracer (cross-shore D integral), and thus independent of absolute concentration. The surface-center of mass μ is the D first moment [*Clark et al.*, 2010]

$$\mu(y)=\frac{\int_{x_{\mathrm{out}}}^{x_{\mathrm{in}}} xD(x,y)\,dx}{\int_{x_{\mathrm{out}}}^{x_{\mathrm{in}}} D(x,y)\,dx}, \tag{3}$$

where x_{out}, the offshore extent of the observed transects, varied from -105 to -298 m over all transects. The jet ski always drove seaward until dye concentrations were not detectable. The model x_{out} is taken at the seaward tracer boundary.

Surfzone bulk cross-shore diffusivity κ_{xx} is estimated using the surfzone-specific squared cross-shore length scale σ^2_{surf}, a shoreline based second moment [*Clark et al.*, 2010]

$$\sigma^2_{\mathrm{surf}}(y)=\frac{\int_{-L_x}^{x_{\mathrm{in}}} x^2D(x,y)dx}{\int_{-L_x}^{x_{\mathrm{in}}} D(x,y)dx}, \tag{4}$$

integrated from the seaward extent of the surfzone $x=-L_x$ (at the location of maximum H_{s}) to $x=x_{\mathrm{in}}$. The H_{s} were modeled with high skill [Part-1], thus modeled and observed L_x are

similar (12 m rms difference). However, the H_s are observed at discrete locations (roughly 20 m apart) resulting in coarse L_x resolution. For comparisons, the observed L_x are used in (4) to estimate model and observed $\sigma^2_{\rm surf}$. The shoreline based (i.e., without subtracting μ) moment $\sigma^2_{\rm surf}$ is appropriate for estimating κ_{xx} near a boundary, assuming the alongshore plume axis is parallel to the shoreline, i.e., no large scale cross-shore advection of the mean plume [*Clark et al.*, 2010].

For each release, a bulk κ_{xx} is estimated from transects that are well contained in the surfzone, thus not effected by smaller diffusivities seaward of the surfzone. Transects are defined as well contained in the surfzone when $\mathcal{R} < 0.55$, where $\mathcal{R}$ is the ratio of plume $\sigma^2_{\rm surf}$ to the $\sigma^2_{\rm surf}$ for a cross-shore uniform tracer concentration [*Clark et al.*, 2010]. For each release, the bulk κ_{xx} is

$$\sigma^2_{\rm surf} = 2\kappa_{xx} t_{\rm p} + \beta, \tag{5}$$

where κ_{xx} and β are fit constants. The plume alongshore advection time

$$t_{\rm p} = \overline{V}^{-1} y, \tag{6}$$

is the approximate plume age at a downstream location y, where the overbar represents a surfzone-average (cross-shore average over the surfzone). The observed $\overline{V}$ are estimated using the cross-shore array of current meters [*Clark et al.*, 2010], and the model $\overline{V}$ is averaged over the surfzone ($-L_x < x < 0$) and the alongshore region between the release location $y = 0$ and the farthest downstream location where κ_{xx} is estimated ($\mathcal{R} < 0.55$). The Fickian solutions used to derive (5) assume constant depth, however numerical solutions to the depth varying case have similar surface tracer moments (i.e., (3) and (4)) and the resulting κ_{xx} are within 10% of the constant depth estimates [*Clark et al.*, 2010]. The observed R1 plume differs from the other releases because the plume moved seaward and did not interact strongly with the shoreline

(Figure 4a, and *Clark et al.* [2010]). Thus, the observed R1 $\kappa_{xx}^{(obs)}$ is estimated from the squared cross-shore length scale σ^2, where the cross-shore advection is removed [for details see *Clark et al.*, 2010].

5.2. Surface center of mass μ

For all releases, the observed $\mu^{(obs)}$ and modeled $\mu^{(A,B,C)}$ generally move seaward at an approximately constant rate with increasing downstream distance y, for $y < 300$ m (Figure 6). The downstream evolution of $\mu^{(obs)}$ and $\mu^{(A,B,C)}$ are similar for R2, R3, and R4 (Figure 6b,c,d). The R1 $\mu^{(obs)}$ and $\mu^{(A,B,C)}$ are similar at the closest transect to the source (Figure 6a), but $\mu^{(obs)}$ magnitudes are slightly larger than $\mu^{(A,B,C)}$ for the two farthest downstream transects, consistent with seaward advection of the observed R1 plume (Figure 4a), possibly by unresolved local bathymetric variation [*Clark et al.*, 2010]. The R6 modeled $\mu^{(C)}$ closely match the $\mu^{(obs)}$, but $\mu^{(A)}$ and $\mu^{(B)}$ magnitudes are generally larger than the $\mu^{(obs)}$, with more alongshore variation in $\mu^{(A)}$ and $\mu^{(B)}$ than $\mu^{(obs)}$. The disparity corresponds with small patches of $D^{(A)}$ ($x < -88$ m, Figure 2f) and $D^{(B)}$ seaward of the surfzone. In R4 and R6 where the plume was measured farther downstream ($y > 300$ m), the rate that μ moves away from the shoreline decreases (Figure 6d,e) presumably owing to weaker mixing seaward of the surfzone. The $\mu^{(A,B,C)}$ skill, $1 - \langle(\mu^{(obs)}(y) - \mu^{(A,B,C)}(y))^2\rangle_y / \langle\mu^{2\,(obs)}(y)\rangle_y$, is estimated for each tracer and release. The mean $\mu^{(A,B,C)}$ skill over all releases and tracers is 0.88 indicating good model-data agreement.

5.3. Cross-shore dispersion and κ_{xx}

The model $\sigma_{surf}^{2\,(A,B,C)}$ and observed $\sigma_{surf}^{2\,(obs)}$ plume squared cross-shore length scales (4) increase with increasing plume alongshore advection time t_p (6), and are qualitatively well modeled for R2, R3, R4, and R6 (Figure 7b,c,d,e). The initial increase in $\sigma_{surf}^{2\,(A,B,C)}$ and $\sigma_{surf}^{2\,(obs)}$ is

roughly linear in $t_{\rm p}$ (Figure 7) consistent with Brownian diffusion regimes. The $\sigma^{2\,(\rm A,B,C)}_{\rm surf}$ skill, $1-\langle(\sigma^{2\,(\rm obs)}_{\rm surf}(t_{\rm p})-\sigma^{2\,(\rm A,B,C)}_{\rm surf}(t_{\rm p}))^2\rangle_{t_{\rm p}}/\langle(\sigma^{2\,(\rm obs)}_{\rm surf}(t_{\rm p}))^2\rangle_{t_{\rm p}}$, averaged over releases R2, R3, R4, and R6 is 0.92. For the purpose of comparison, the R1 $\sigma^{2\,(\rm obs)}(t_{\rm p})$ is compared with the modeled $\sigma^{2\,(\rm A,B,C)}_{\rm surf}(t_{\rm p})-\langle\sigma^{2\,(\rm A,B,C)}_{\rm surf}(t_{\rm p}=0)\rangle_{\rm A,B,C}$ (Figure 7a). The R1 modeled and observed squared cross-shore length scales evolve similarly (Figure 7a), but this comparison is qualitative and skill is not estimated.

Mean modeled cross-shore surfzone diffusivities $\langle\kappa_{xx}\rangle_{\rm A,B,C}$ (averaged across tracers A, B, and C) are estimated by least squares fits (5) where the tracer plumes are surfzone contained ($\mathcal{R}<0.55$, below the dashed gray lines in Figure 7). The R1 $\kappa^{(\rm obs)}_{\rm xx}$ is a special case discussed in *Clark et al.* [2010]. Linear fits to $\sigma^{2\,(\rm A,B,C)}_{\rm surf}$ versus $t_{\rm p}$ have high r^2 values, with a mean $r^2=0.87$. The $\langle\kappa_{xx}\rangle_{\rm A,B,C}$ errors are derived in the same manner as the observations [*Clark et al.*, 2010], and include uncertainties in $\sigma^{2\,(\rm A,B,C)}_{\rm surf}$ and the best fit slope [*Wunsch*, 1996]. The $\langle\kappa_{xx}\rangle_{\rm A,B,C}$ range from 0.67–2.83 $\rm m^2\,s^{-1}$(Table 3).

Model $\langle\kappa_{xx}\rangle_{\rm A,B,C}$ and observed $\kappa^{(\rm obs)}_{\rm xx}$ are similar (Figure 8), with correlation $r^2=0.72$. The skill, $1-\langle(\kappa^{(\rm obs)}_{\rm xx}-\langle\kappa_{xx}\rangle_{\rm A,B,C})^2\rangle_{\rm R1-R6}/\langle(\kappa^{(\rm obs)}_{\rm xx})^2\rangle_{\rm R1-R6}$, is 0.40. Model and observed cross-shore dispersion κ_{xx} are qualitatively similar for the given bathymetries and incident wave fields.

6. Discussion

6.1. Model-data comparison

6.1.1. Mean plume concentration D and alongshore transport M

The magnitude and cross-shore structure of tracer concentration $D^{(\rm A,B,C)}$ is more difficult to model than cross-shore integrated, normalized moments (μ and $\sigma^2_{\rm surf}$), because $D^{(\rm A,B,C)}$ depends on the details of $V(x)$, eddy stirring, and the input tracer flux. Model and observed $D^{(\rm A)}$ and $D^{(\rm obs)}$ are similar with good skill (0.5–0.73) for releases R3, R4, and R6 (Figure 4c,d,e),

where the waves, $V(x)$, and eddy velocities were also well modeled [Part-1]. However, other releases have significant deviations in plume location (R1, Figure 4a) or tracer magnitude (R2, Figure 4b) leading to low (negative) $D^{(\mathrm{A})}$ skill. The difference in R1 cross-shore plume location likely results from cross-shore advection of the mean $D^{(\mathrm{obs})}$ plume (i.e., the along-plume axis is not parallel to shore). The R2 $D^{(\mathrm{A})}$ are reasonably matched in the outer surfzone ($x < -60$ m, Figure 4b), but $D^{(\mathrm{A})}$ magnitudes are often 2-5 times greater than $D^{(\mathrm{obs})}$ near the shoreline, contrasting with the good agreement between R2 $M^{(\mathrm{A,B,C})}$ and $M^{(\mathrm{obs})}$ tracer transports (Figure 5b). Near the shoreline, the R2 model $V \approx 0.05\ \mathrm{m\,s^{-1}}$substantially underpredicts the observed $V \approx 0.3\ \mathrm{m\,s^{-1}}$[Figure 6, Part 1], but combined with the over-predicted $D^{(\mathrm{A})}$ (Figure 4b), results in good M model-data agreement. (Figure 5b).

6.1.2. Cross-shore moments μ and σ^2_{surf}, and diffusivity κ_{xx}

Although $D^{(\mathrm{A,B,C})}$ skill is variable and sometime negative, the normalized cross-shore integrated moments $\mu^{(\mathrm{A,B,C})}$ (3) and $\sigma^{2\,(\mathrm{A,B,C})}_{\mathrm{surf}}$ (4), representing cross-shore plume structure, have high mean skill (0.88 and 0.92, respectively). For example, despite low $D^{(\mathrm{A,B,C})}$ skill, R2 has high $\mu^{(\mathrm{A,B,C})}$ skill (Figure 6b) and the best agreement (highest $\sigma^{2\,(\mathrm{A,B,C})}_{\mathrm{surf}}$ skill) with the observed cross-shore dispersion (Figure 7b). This is in part due to scaling the model and observations with t_{p} which reduces the sensitivity to R2 $V(x)$ model errors. Thus cross-shore diffusivities κ_{xx} may still be accurately modeled when $V(x)$ and $D^{(\mathrm{A,B,C})}$ are not.

Drifter observations indicate ballistic dispersion ($\sigma^2 \propto t^2$) for times $\lessapprox 50$ s and brownian dispersion at longer times [*Spydell et al.*, 2009]. Tracer observations were generally at downstream distances corresponding to $t_{\mathrm{p}} > 100$ s [*Clark et al.*, 2010], and the observed and the modeleded σ^2_{surf} are consistent with Brownian diffusion ($\sigma^2 \propto t$, Figure 7). At short times (where there are no observations), a ballistic dispersion regime is not apparent in the model $\sigma^{2\,(\mathrm{A,B,C})}_{\mathrm{surf}}$, poten-

tially because of a mix of background diffusivity, bore-mixing, and eddy stirring which all have different time-scales.

Model $\langle \kappa_{xx} \rangle_{\mathrm{A,B,C}}$ and observed $\kappa_{\mathrm{xx}}^{(\mathrm{obs})}$ are similar with correlation $r^2 = 0.72$ and moderate 0.40 skill (Figure 8). Thus, given only the bathymetry and incident wave field, the coupled Boussinesq-tracer model qualitatively reproduces the observed cross-shore absolute tracer dispersion and suggests that the model can be used to study the mechanisms of surfzone tracer dispersion.

6.1.3. R6 dispersion, seaward of the surfzone

The R6 $\mu^{(\mathrm{C})}$ closely matches $\mu^{(\mathrm{obs})}$, but $\mu^{(\mathrm{A})}$ and $\mu^{(\mathrm{B})}$ are farther seaward, resulting in the lowest $\mu^{(\mathrm{A,B,C})}$ mean skill (0.68) of all releases. Despite the highest $D^{(\mathrm{A,B,C})}$ skill (Table 2), low concentrations of $D^{(\mathrm{A})}$ and $D^{(\mathrm{B})}$ extend much farther seaward than the $D^{(\mathrm{obs})}$ (see Figure 4e for $D^{(\mathrm{A})}$), thus increasing $\mu^{(\mathrm{A})}$ and $\mu^{(\mathrm{B})}$ magnitudes. This may indicate model mixing rates seaward of the surfzone are larger, or have different structure, than observed. Seaward of the surfzone, vertical tracer structure, not accounted for here, may also become important [e.g., *Kim and Lynett*, 2010].

6.1.4. Potential sources of error

The variation between modeled individual tracer (A,B,C) statistics (e.g., $\sigma_{\mathrm{surf}}^{2\,(\mathrm{A,B,C})}$, Figure 7) is due to two factors. First, small alongshore variations in the surfzone eddy field [e.g., Part-1, Figures 14 and 15] result in each tracer experiencing different stirring statistics. In addition, the velocity field stirring tracer has a red spectrum [Part-1, Figure 13], and averaging for 8000 s is not sufficient to not sufficient to converge tracer statistics from the three release locations. The red spectrum of the velocity field may be intrinsic, as part of 2D turbulence, or may be an artifact of the model wavemaker [e.g., *Johnson and Pattiaratchi*, 2006].

The observed $\kappa_{xx}^{(obs)}$ estimates assume $\sigma_{surf}^{2\,(obs)}(t_p = 0) = x_{rl}^2$ (tracer δ-function at the release location). However, the model $\sigma_{surf}^{2\,(A,B,C)}(t_p = 0)$ for R2, R3, and R4 are larger (by 153–724 m^2) than the assumed x_{rl}^2 value for the observations (Figure 7b,c,d). The elevated model $\sigma_{surf}^{2\,(A,B,C)}$ relative to x_{rl}^2 is due to intermittent model tracer recirculation upstream of the tracer source (e.g.,Figure 2a), and consistent with visual observations. Additional model experiments with non-breaking waves on a steady current demonstrate that cross-shore tracer dispersion due to orbital wave motions is weak and contributes only a small fraction of the model $\sigma_{surf}^{2\,(A,B,C)}$ near $y = 0$ m. The assumed $\sigma_{surf}^{2\,(obs)}(t_p = 0) = x_{rl}^2$ likely underestimates the actual value, and the observed fit slopes (5) and $\kappa_{xx}^{(obs)}$ may be slightly overestimated.

6.2. Alongshore tracer transport: eddy fluxes and cross-shore integration limits

For equilibrated conditions ($t > 6000$ s, Figure 3) and conserved tracer, the time averaged alongshore tracer transport is expected to be constant downstream of the source. However, the model and observed M (2) are not conserved, do not match the input flux, and vary downstream by up to 50% (Figure 5). Model and observed tracer transports M are both estimated using time-averaged D and V (2), excluding alongshore eddy fluxes, and neglect the regions onshore of x_{in} and offshore of x_{F7}. The time-averaged total alongshore tracer transport $\mathcal{M}(y)$ is estimated with

$$\mathcal{M}(y) = \int_{x_{F7}}^{x_{in}} \langle [h(x) + \eta(x,y,t)]\, v(x,y,t)\, d(x,y,t) \rangle_t \, dx, \tag{7}$$

where v and d are the instantaneous model alongshore velocity and tracer concentration, respectively, and the time-averaged $\langle [h + \eta]\, v\, d \rangle_t$ includes both mean and eddy alongshore tracer fluxes. The $x_{in} < x < x_{F7}$ integral limits are used for comparison with $M^{(A,B,C)}$ (2). The R4 $\mathcal{M}^{(A)}$, representative of other tracers and releases, matches the input flux at $y = 0$ and varies

less downstream than $M^{(\mathrm{A})}$ (Figure 9). The $\mathcal{M}^{(\mathrm{A})}$ and $M^{(\mathrm{A})}$ have roughly similar magnitudes, indicating small alongshore eddy fluxes, consistent with the assumptions used to derive κ_{xx} (5).

A domain integrated total transport estimate $\mathcal{M}^{(\mathrm{A})}_{\mathrm{domain}}$ is defined similarly to (7) but integrated over the entire cross-shore tracer domain (Figure 1). The $\mathcal{M}^{(\mathrm{A})}_{\mathrm{domain}}$ decreases less downstream than $M^{(\mathrm{A})}$ and $\mathcal{M}^{(\mathrm{A})}$ (Figure 9). The $\mathcal{M}^{(\mathrm{A})}$ are initially ($y < 100$ m) smaller than $\mathcal{M}^{(\mathrm{A})}_{\mathrm{domain}}$ because $\mathcal{M}^{(\mathrm{A})}$ excludes tracer shoreward of x_{in}. The $\mathcal{M}^{(\mathrm{A})}$ are also smaller farther downstream ($y > 200$ m) because tracer transport seaward of x_{F7} is excluded. The downstream decrease in $\mathcal{M}^{(\mathrm{A})}_{\mathrm{domain}}$ is due to tracer losses at the offshore boundary, indicating that a larger cross-shore domain, in addition to incorporating the effects of vertical variation of tracer and currents and stratification, are needed to study tracer evolution seaward of the surfzone.

6.3. Simple Fickian Equation Comparison: Tracer Maxima

Cross-shore diffusivity κ_{xx} is estimated here and in *Clark et al.* [2010] using a simple Fickian solution, where the tracer cross-shore maxima decrease downstream as $D_{\max} \sim t_{\mathrm{p}}^{-1/2}$ [*Clark et al.*, 2010]. The individual $D^{(\mathrm{A,B,C})}_{\max}$ model tracers are similar, and the mean $[\langle D\rangle_{\mathrm{A,B,C}}]_{\max}$ over tracers A, B, and C is compared with the expected $t_{\mathrm{p}}^{-1/2}$ dependence over the surfzone contained region where κ_{xx} is estimated.

The R1, R4, and R6 $[\langle D\rangle_{\mathrm{A,B,C}}]_{\max}$ decrease similarly to $t_{\mathrm{p}}^{-1/2}$ (Figure 10). The R2 and R3 $[\langle D\rangle_{\mathrm{A,B,C}}]_{\max}$ initially ($t_{\mathrm{p}} < 200$ s) decrease similarly to $t_{\mathrm{p}}^{-1/2}$, but decrease more rapidly with $t_{\mathrm{p}} > 200$ s (Figure 10), possibly because tracer is leaking into deeper water seaward of the surfzone. Linear regressions of the form $[\langle D\rangle_{\mathrm{A,B,C}}]_{\max} = At^{-\gamma}$, with A and γ fit constants, yield γ slightly greater than 0.5. The similarity between $[\langle D\rangle_{\mathrm{A,B,C}}]_{\max}$ and $t_{\mathrm{p}}^{-1/2}$ indicates that (5) is appropriate for estimating κ_{xx}, and that the modeled absolute diffusion is generally well represented by a simple Fickian equation, when the tracer is well contained within the surfzone.

Diffusivities estimated from $[\langle D\rangle_{\mathrm{A,B,C}}]_{\max}$ versus t_{p} (not shown) are similar to those estimated from $\sigma_{\mathrm{surf}}^{2\,(\mathrm{A,B,C})}$, but are much noisier and include uncertainties in the absolute tracer concentration.

6.4. Tracer dispersion induced by breaking wave κ_{br}

For time-averaged breaking-wave (bore) induced diffusion, scalings similar to $\kappa_{xx} \propto H_{\mathrm{s}}^2 T_{\mathrm{m}}^{-1}$, were suggested by several previous studies [*Harris et al.*, 1963; *Inman et al.*, 1971; *Clarke et al.*, 2007; *Feddersen*, 2007; *Henderson*, 2007], but had lower skill (0.32) than alternate scalings and best fit slope smaller than expected when applied to the HB06 observed κ_{xx} [*Clark et al.*, 2010]. The relative importance of simulated bore diffusion is investigated for the modeled HB06 tracer plumes.

Tracer mixing by breaking waves is modeled with a breaking eddy diffusivity κ_{br} (set equal to the local breaking eddy viscosity ν_{br}), which propagates with the front face of a breaking wave (bore) [*Feddersen*, 2007]. In the absence of other dispersion mechanisms, a tracer patch that is much wider than the cross-shore width of a bore (approximately the water depth) has a bulk cross-shore diffusivity given by the time-averaged breaking diffusivity $\langle\kappa_{\mathrm{br}}\rangle_t$ [*Henderson*, 2007].

The R4 $\langle\kappa_{\mathrm{br}}\rangle_t$ increases from zero, far seaward of the surfzone, to a maxima near the outer-surfzone ($x \approx -100$ m), and then decreases towards the shoreline (Figure 11). Although R4 has the largest breaking diffusivities of all releases, the maximum $\langle\kappa_{\mathrm{br}}\rangle_t = 0.06\ \mathrm{m^2\,s^{-1}}$ is much smaller than the $O(1)$ estimates for $\langle\kappa_{xx}\rangle_{\mathrm{A,B,C}}$ (Figure 8 and Table 3), suggesting the effect of bore-mixing [*Feddersen*, 2007] on absolute averaged tracer properties is weak.

The weak effect of breaking wave induced κ_{br} on cross-shore absolute dispersion is demonstrated by an additional R4 simulation with two tracers released at the same location, one with

breaking and background diffusivities $\kappa_{\rm br} + \kappa_0$ and another with only background κ_0 applied to the tracer field. The R4 model $\sigma^2_{\rm surf}$ with and without $\kappa_{\rm br}$ are almost identical (Figure 12, other releases are similar), demonstrating that model bore-induced mixing is insignificant to bulk surfzone cross-shore dispersion for the obliquely incident, directionally spread wave conditions modeled here.

6.5. Model mixing-length κ_{xx} scalings

A mixing-length scaling for the cross-shore diffusivity

$$\kappa_{xx} \propto \overline{\mathcal{V}}^{\rm (IG)}_{\rm rot}\, L_x, \tag{8}$$

was compared with observed diffusivities, where $\overline{\mathcal{V}}^{\rm (IG)}_{\rm rot}$ is a surfzone-averaged infragravity horizontal rotational velocity (estimated following [*Lippmann et al.*, 1999], and discussed in [Part-1]) and L_x is the surfzone width [*Clark et al.*, 2010]. This scaling (8) was correlated ($r^2 = 0.59$) with observed $\kappa^{\rm (obs)}_{\rm xx}$, and suggested that stirring by infragravity (IG, $0.004 < f < 0.03$ Hz) eddies (vortical motions) was a significant cross-shore tracer dispersion mechanism. In addition, note that although $\kappa^{\rm (obs)}_{\rm xx}$ was also correlated with $\overline{V}\, L_x$, $\overline{V}$ appeared in the formulation for $\kappa^{\rm (obs)}_{\rm xx}$ and the correlation could be artificially high. The observed IG-band rotational velocities $\mathcal{V}^{\rm (IG)}_{\rm rot}(x)$ were well reproduced by the model [see Figure 14, Part-1]. Here, the mixing-length scaling (8) is investigated for the modeled dispersion.

The model $\overline{\mathcal{V}}^{\rm (IG)}_{\rm rot}$ are estimated by cross-shore averaging the model $\mathcal{V}^{\rm (IG)}_{\rm rot}(x)$ over the surfzone ($-L_x < x < 0$). Over the five releases, the model $\langle \kappa_{xx} \rangle_{\rm A,B,C}$ and $\overline{\mathcal{V}}^{\rm (IG)}_{\rm rot} L_x$ are related (Figure 13a), with a best fit slope of 0.1. This slope is near the observed best fit slope of 0.2 suggesting that this scaling is also applicable in the model. However, the squared correlation $r^2 = 0.29$ is lower than observed ($r^2 = 0.59$). The scaling is not expected to represent all the

dispersive processes in the surfzone, and the diffusivity is expected to be non-zero (and positive) when $\overline{\mathcal{V}}_{\rm rot}^{\rm (IG)} L_x = 0$. The positive best fit y-intercept (Figure 14a) is roughly consistent with this expectation.

Observed and modeled very low frequency (VLF, $f < 0.004$ Hz) contributions to the bulk rotational velocity estimate [Figure 15, Part-1], not considered in *Clark et al.* [2010], have similar magnitudes to those in the IG-band [Figure 14, Part-1], and may represent a significant contribution to cross-shore mixing. A mixing-length scaling $\kappa_{xx} \sim \overline{\mathcal{V}}_{\rm rot}^{\rm (IG+VLF)} L_x$ similar to (8), using a surfzone averaged horizontal rotational velocity $\overline{\mathcal{V}}_{\rm rot}^{\rm (IG+VLF)}$ integrated over both IG and VLF frequency bands ($0.001 < f < 0.03$ Hz), is tested for the model. The $\overline{\mathcal{V}}_{\rm rot}^{\rm (IG+VLF)} L_x$ scaling has a best fit slope of 0.06, and a higher correlation ($r^2 = 0.60$) with $\langle \kappa_{xx} \rangle_{\rm A,B,C}$ (compare Figure 13b with Figure 13a), indicating that VLF motions are likely important to model cross-shore tracer dispersion in the surfzone. The best fit y-intercept is near zero, similar to $\overline{\mathcal{V}}_{\rm rot}^{\rm (IG)} L_x$. The model rotational motions in the VLF frequency band are roughly twice the observed velocities, thus VLF motions may be more important to tracer dispersion in the model than in the field.

Estimates of rotational velocities using a collocated pressure and velocity measurement [*Lippmann et al.*, 1999] are useful for field applications, but involve assumptions about the low frequency wave field. More accurate and complete rotational velocities are estimated by decomposing the model instantaneous velocity field into rotational $\boldsymbol{u}_\psi$ and irrotational $\boldsymbol{u}_\phi$ components [e.g., *Spydell and Feddersen*, 2009, and Part-1], where model vorticity comes entirely from the rotational $\boldsymbol{u}_\psi$. The majority of contributions to $\boldsymbol{u}_\psi$ are in the IG and VLF frequency bands [Figure 13, Part-1].

While $\overline{\mathcal{V}}_{\rm rot}^{\rm (IG+VLF)}$ combines both cross- and alongshore rotational motions, only the cross-shore component of the rotational velocity field (i.e., u_ψ) is expected to mediate cross-shore

dispersion. A bulk cross-shore rotational velocity $\overline{U}_{\psi}^{(\mathrm{rms})}$, estimated from the surfzone averaged rms model cross-shore rotational velocities u_{ψ}, is applied to the scaling, i.e., $\kappa_{xx} \propto \overline{U}_{\psi}^{(\mathrm{rms})} L_x$. This scaling has a squared correlation $r^2 = 0.63$ (Figure 13c), similar to the $\overline{\mathcal{V}}_{\mathrm{rot}}^{(\mathrm{IG+VLF})}$ squared correlation, and a best fit slope of 0.1. The best fit y-intercept is negative, but close to zero. This scaling again suggests that VLF motions are an important factor in model dispersion.

Unlike the diffusivity scalings and simple Fickian solutions (best fits to κ_{xx} and σ^2_{surf}, respectively) the Boussinesq model is not tuned to match tracer statistics. Given the similarity between model and observed tracer dispersion, the model can give insight into tracer dispersion mechanisms and improve the skill and reliability (over a range of beach and wave conditions) of diffusivity scalings. Improved scalings may provide the rapid (albeit approximate) estimates needed to predict pollutant dispersal in an emergency.

7. Summary

A time-dependent wave-resolving Boussinesq surfzone model `funwaveC`, coupled with a tracer advection diffusion equation, is used to simulate 5 tracer releases from the HB06 experiment. The model, using the observed bathymetry and incident wave spectra, reproduces the cross-shore evolution of significant wave height, mean alongshore currents, and low frequency rotational motions, i.e., eddies [Part-1]. Model tracer is transported by currents, stirred by eddies, and mixed with a breaking wave eddy diffusivity κ_{br}, and a small ($0.01\ \mathrm{m^2\,s^{-1}}$) background diffusivity. Three non-interacting model tracers were released 250 m apart in the alongshore at the rates and cross-shore release locations of the observations.

Similar to the observations, the continuously released model tracers form alongshore parallel plumes in the wave-driven alongshore current, with decreasing peak concentrations and increasing cross-shore widths with downstream distance from the source. Modeled $D^{(\mathrm{A,B,C})}$

and observed $D^{(\mathrm{obs})}$ mean tracer profiles are often shoreline attached (near-shoreline maxima). Three releases (R3, R4, and R6) have high D skill (0.5–0.73) with well matched plumes. Two releases (R1, R2) have negative skill, associated with a mismatch in plume cross-shore location (R1), or differences in the modeled and observed mean alongshore current near the shoreline (R2).

The modeled alongshore tracer transport M agrees with the data for most releases, but is overestimated for R3. Small tracer losses at the seaward model boundary do not effect surfzone dispersion results, but indicate a much larger cross-shore domain would be required to examine processes seaward of the surfzone. Alongshore tracer eddy fluxes are small, and in agreement with neglecting alongshore tracer dispersion in cross-shore diffusivity estimates.

The observed and modeled cross-shore integrated moments, normalized to remove the dependence on absolute concentration, agree well for all releases. The model $D^{(\mathrm{A,B,C})}$ surface-centers of mass $\mu^{(\mathrm{A,B,C})}$ move seaward with downstream distance, and agree well with observations (0.88 skill over all releases). The plume squared cross-shore length scale σ^2_{surf} (second moment) is used to estimate bulk cross-shore diffusivity κ_{xx}. The downstream evolution of model and observed σ^2_{surf} is similar, with high skill (0.92).

Mean model $\langle\kappa_{xx}\rangle_{\mathrm{A,B,C}}$ are similar to observed $\kappa^{(\mathrm{obs})}_{\mathrm{xx}}$, with good correlation ($r^2 = 0.72$) and skill of 0.40. Observed $\kappa^{(\mathrm{obs})}_{\mathrm{xx}}$ were correlated with a mixing-length scaling based on bulk infragravity (IG) cross-shore rotational velocities $\overline{\mathcal{V}}^{(\mathrm{IG})}_{\mathrm{rot}}$, however modeled $\langle\kappa_{xx}\rangle_{\mathrm{A,B,C}}$ have lower correlation ($r^2 = 0.29$) with this scaling. Alternative mixing-length scalings including both IG and very low frequency (VLF, $f < 0.004$ Hz) rotational motions, have higher $r^2 = 0.60 - 0.63$ correlations with $\langle\kappa_{xx}\rangle_{\mathrm{A,B,C}}$. The mean model wave-breaking eddy diffusivity is small and does not effect the bulk dispersion significantly.

The good overall agreement between model and observed tracer plume properties indicates that, given the bathymetry and incident wave field, coupled time-dependent Boussinesq and tracer models can be used to predict surfzone mean tracer evolution and are appropriate for studying the mechanisms of surfzone tracer dispersion.

Acknowledgments. This research was supported by SCCOOS, CA Coastal Conservancy, NOAA, NSF, ONR, and CA Sea Grant. Staff, students, and volunteers from the Integrative Oceanography Division (B. Woodward, B. Boyd, K. Smith, D. Darnell, I. Nagy, M. Okihiro, M. Omand, M. Yates, M. McKenna, M. Rippy, S. Henderson, D. Michrokowski) were instrumental in acquiring the field observations. We thank these people and organizations.

References

Clark, D. B., F. Feddersen, M. M. Omand, and R. T. Guza, Measuring fluorescent dye in the bubbly and sediment laden surfzone, *Water Air Soil Poll.*, *204*(1-4), 103–115, doi: 10.1007/s11270-009-0030-z, 2009.

Clark, D. B., F. Feddersen, and R. T. Guza, Cross-shore surfzone tracer dispersion in an alongshore current, *J. Geophys. Res., Oceans*, *115*(C10035), doi:10.1029/2009JC005683, 2010.

Clarke, L. B., D. Ackerman, and J. Largier, Dye dispersion in the surfzone: Measurements and simple models, *Cont. Shelf Res.*, *27*, 650–669, 2007.

Csanady, G. T., *Turbulent Diffusion in the Environment*, D. Reidel, New York, 1973.

Feddersen, F., Breaking wave induced cross-shore tracer dispersion in the surfzone: Model results and scalings, *J. Geophys. Res.*, *112*(C09012), doi:10.1029/2006JC004006, 2007.

Feddersen, F., Observations of the surfzone dissipation rate, *J. Phys. Ocean.*, submitted, 2011.

Feddersen, F., and J. H. Trowbridge, The effect of wave breaking on surf-zone turbulence and alongshore currents: A modeling study, *J. Phys. Ocean.*, *35*, 2187–2204, 2005.

Feddersen, F., D. B. Clark, and R. T. Guza, Boussinesq modeling of surfzone tracer plumes, Part 1: Eulerian wave and current comparisons, *J. Geophys. Res.*, submitted, 2011.

Geiman, J. D., J. T. Kirby, A. J. H. M. Reniers, and J. H. MacMahan, Effects of wave-averaging on estimates of fluid mixing in the surf zone, *J. Geophys. Res.*, *in press*, 2011.

Harris, T. F. W., J. M. Jordaan, W. R. McMurray, C. J. Verwey, and F. P. Anderson, Mixing in the surf zone, *Int. J. Air Wat. Polut.*, *7*, 649–667, 1963.

Henderson, S. M., Comment on 'Breaking wave induced cross-shore tracer dispersion in the surfzone: Model results and scalings', *J. Geophys. Res.*, *111*(C12007), doi: 10.1029/2006JC003539, 2007.

Inman, D. L., R. J. Tait, and C. E. Nordstrom, Mixing in the surfzone, *J. Geophys. Res.*, *26*, 3493–3514, 1971.

Issa, R., D. Rouge, M. Benoit, D. Violeau, and A. Joly, Modelling algae transport in coastal areas with a shallow water equation model including wave effects, *J. Hydro-environ. Res.*, *3*(4), 1570–6443, doi:10.1016/j.jher.2009.10.004, 2010.

Johnson, D., and C. Pattiaratchi, Boussinesq modelling of transient rip currents, *Coastal Eng.*, *53*(5), 419–439, 2006.

Kim, D.-H., and P. J. Lynett, Turbulent mixing and passive scalar transport in shallow flows, *Phys. Fluids*, *23*(016603), doi:10.1063/1.3531716, 2010.

Lippmann, T. C., T. H. C. Herbers, and E. B. Thornton, Gravity and shear wave contributions to nearshore infragravity motions, *J. Phys. Ocean.*, *29*(2), 231–239, 1999.

Nwogu, O., Alternative form of Boussinesq equations for nearshore wave propagation, *J. Wtrwy., Port, Coast., and Oc. Engrg.*, *119*, 618–638, 1993.

Pearson, J. M., I. Guymer, J. R. West, and L. E. Coates, Solute mixing in the surf zone, *J. Waterwy., Port, Coast., and Oc. Eng.*, *135*(4), 127–134, 2009.

Peregrine, D. H., Long waves on a beach, *J. Fluid Mech.*, *27*(04), 815–827, doi: 10.1017/S0022112067002605, 1967.

Peregrine, D. H., Surf zone currents, *Theor. Comput. Fluid Dyn.*, *10*, 295–309, 1998.

Rodriguez, A., A. Sánchez-Arcilla, J. Redondo, E. Bahia, and J. Sierra, Pollutant dispersion in the nearshore region: Modelling and measurements, *Wat. Sci. and Tech.*, *32*(9-10), 169–178, doi:doi:10.1016/0273-1223(96)00088-1, 1995.

Ruessink, B. G., Observations of turbulence within a natural surf zone, *J. Phys. Ocean.*, *40*(12), 2696–2712, doi:10.1175/2010JPO4466.1, 2010.

Schmidt, W. E., B. T. Woodward, K. S. Millikan, and R. T. Guza, A GPS-tracked surf zone drifter, *J. Atmos. and Ocean. Tech.*, *20*, 1069–1075, 2003.

Schmidt, W. E., R. T. Guza, and D. N. Slinn, Surf zone currents over irregular bathymetry: Drifter observations and numerical simulations, *J. Geophys. Res.*, *110*, doi: 10.1029/2004JC002421, 2005.

Spydell, M. S., and F. Feddersen, Lagrangian drifter dispersion in the surf zone: Directionally spread, normally incident waves, *J. Phys. Ocean.*, *39*, 809–830, 2009.

Spydell, M. S., F. Feddersen, and R. T. Guza, Observations of drifter dispersion in the surfzone: The effect of sheared alongshore currents, *J. Geophys. Res.*, *114*(C07028, doi:10.1029/2009JC005328), 2009.

557 Tao, S., and T. JianHua, Numerical simulation of pollutant transport acted by wave for a shallow
558 water sea bay, *Int. J. Numer. Meth. Fluids*, *51*, 469–487, doi:10.1002/fld.1116, 2006.
559 Wei, G., J. T. Kirby, S. T. Grilli, and R. Subramanya, A fully nonlinear Boussinesq model for
560 surface waves. I. Highly nonlinear, unsteady waves., *J. Fluid Mech.*, *294*, 71–92, 1995.
561 Wunsch, C., *The Ocean Circulation Inverse Problem*, Cambridge University Press, 1996.

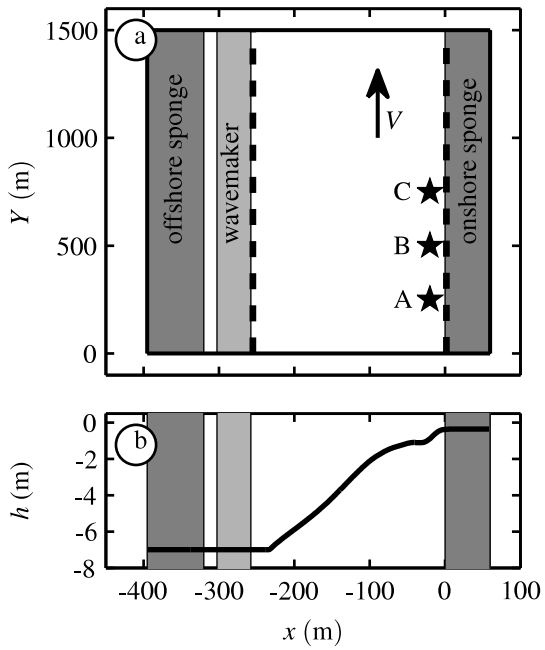

Figure 1. (a) Plan view of a typical model domain (R4 example). The cross-shore distance from the "shoreline" is x, and Y is the alongshore coordinate. Gray regions indicate sponge layers and the wavemaker. The cross-shore tracer domain (dashed lines) is bounded by the offshore wavemaker and the onshore sponge layer. Stars indicate release locations for model tracers A ($Y_{\rm rl} = 250$ m), B ($Y_{\rm rl} = 500$ m), and C ($Y_{\rm rl} = 750$ m), and the arrow indicates the direction of the mean alongshore current V. (b) Typical model cross-shore bathymetry h versus x (R4 example), with a flat region at 7 m depth for the offshore sponge layer and wavemaker and a 0.3 m depth flat region for the onshore sponge layer.

Table 1. Model tracer release parameters: input tracer flux M_0, and cross-shore release location x_{rl}.

Release	M_0 ($\mathrm{ppb\,m^3\,s^{-1}}$)	x_{rl} (m)
R1	263	-54
R2	647	-13
R3	1256	-10
R4	1489	-22
R6	485	-12

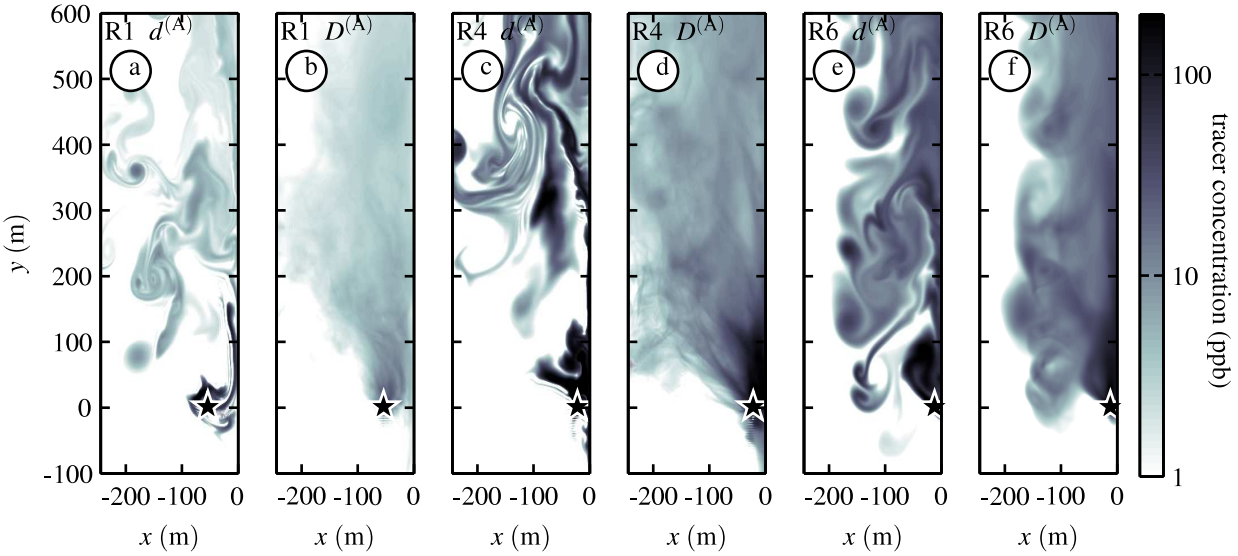

Figure 2. (a, c, e) Instantaneous $d^{(\mathrm{A})}$ and (b, d, f) mean $D^{(\mathrm{A})}$ (time average over 6000–14,000 s after each tracer release begins) modeled tracer A concentration as a function of x, the cross-shore distance from the "shoreline", and y, the alongshore distance from the dye source, for (a, b) R1, (c, d) R4, and (e, f) R6. In each panel the back star indicates the cross-shore release location (x_{rl}, Table 1).

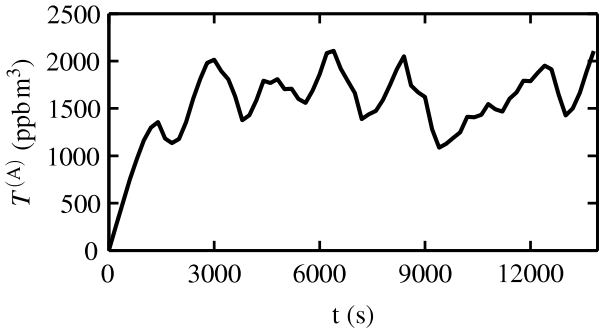

Figure 3. The R4 total tracer A volume $T^{(\mathrm{A})}$ versus time after the tracer release began, where $T^{(\mathrm{A})}(t) = \int\int (h+\eta) d^{(\mathrm{A})}(t)\, dy\, dx$ is integrated over the entire cross-shore tracer domain and from the upstream model boundary to 250 m downstream of the tracer source (where R4 diffusivities are estimated). For $t > 3000$ s the quasi-steady-state $T^{(\mathrm{A})}$ oscillates about a mean. The R4 $T^{(\mathrm{A})}$ is representative of other tracers and releases.

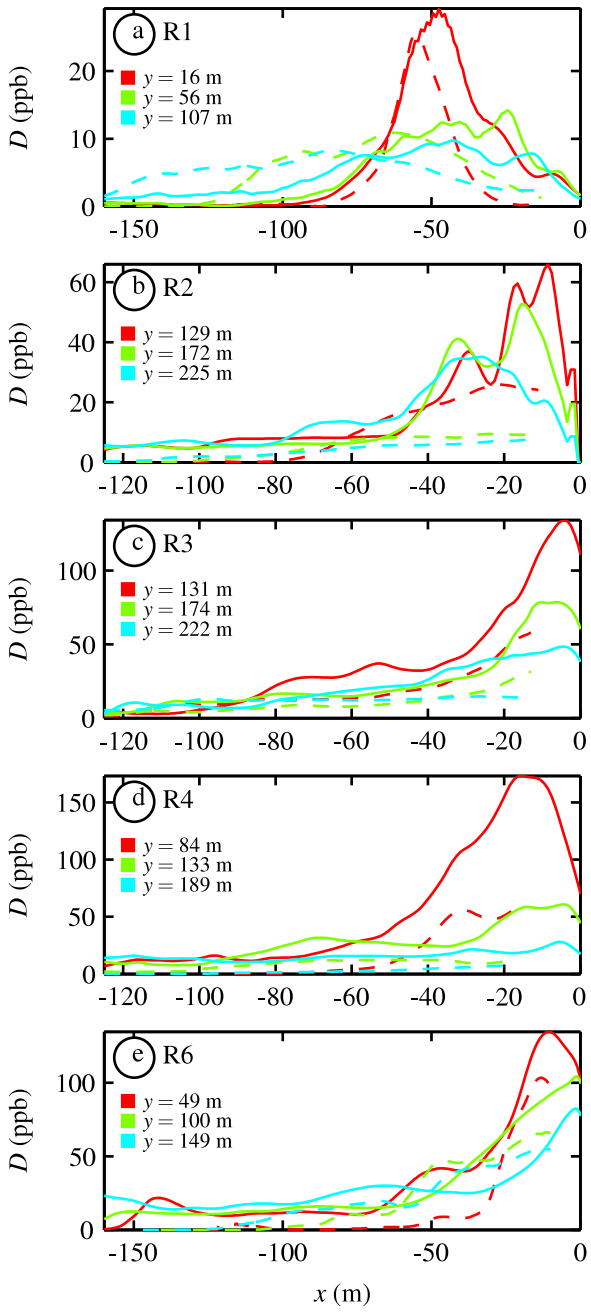

Figure 4. Modeled $D^{(\mathrm{A})}$ (solid) and observed $D^{(\mathrm{obs})}$ (dashed) mean tracer profiles versus x for (a) R1, (b) R2, (c) R3, (d) R4, and (e) R6, with alongshore distance y from the source indicted by the legend in each panel. Observed transects extend from seaward of the tracer plume to the inner transect edge x_{in}.

Table 2. For each release, the mean tracer concentration skill $1 - \langle (D^{(\mathrm{obs})}(x,y) - D^{(\mathrm{A,B,C})}(x,y))^2 \rangle_{x,y} / \langle D^{2\,(\mathrm{obs})}(x,y) \rangle_{x,y}$, averaged over all observed transects where $D^{(\mathrm{obs})} > 5$ ppb and all 3 (A,B,C) model tracers.

R1	R2	R3	R4	R6
-2.70	-8.89	0.70	0.50	0.73

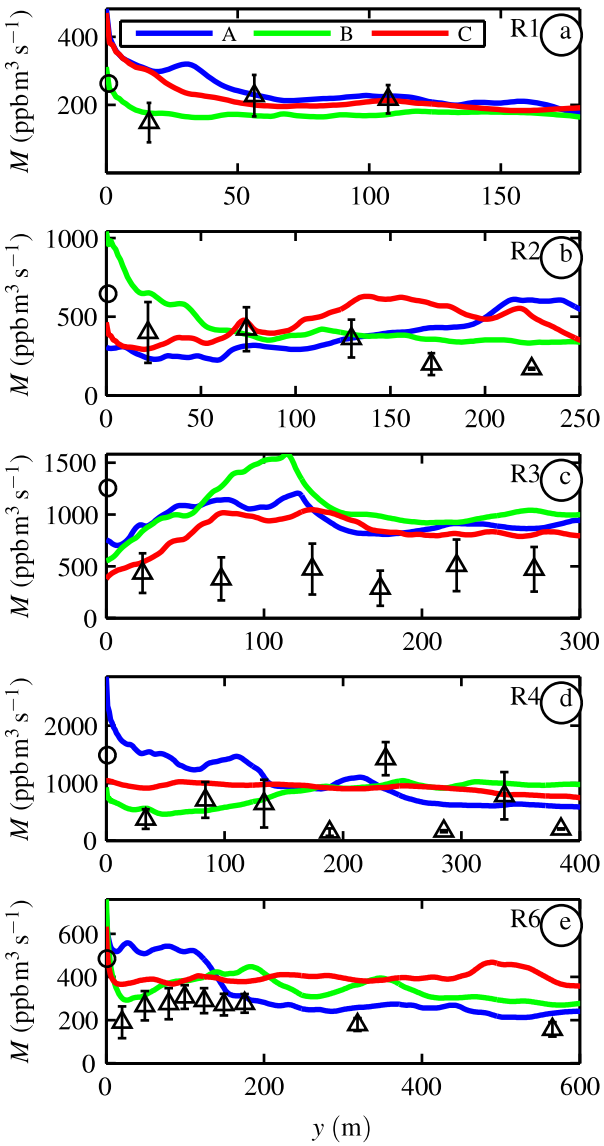

Figure 5. Modeled $M^{(\mathrm{A,B,C})}$ (colored curved) and observed $M^{(\mathrm{obs})}$ (open black triangles with error bars) alongshore tracer transport (2) versus y, for releases (a) R1, (b) R2, (c) R3, (d) R4, and (e) R6. The observed dye release rate is estimated by the open black circle at $y = 0$.

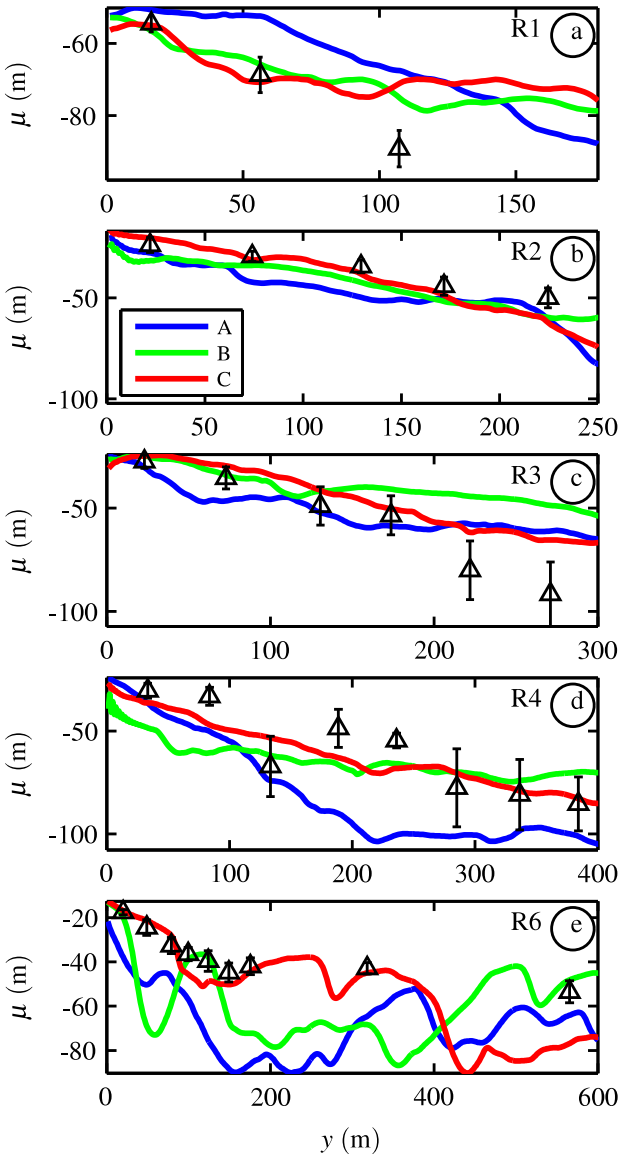

Figure 6. Modeled (colored) and observed (black triangles with error bars) surface center of mass μ versus y for releases (a) R1, (b) R2, (c) R3, (d) R4, and (e) R6. The mean model skill over all releases is 0.88.

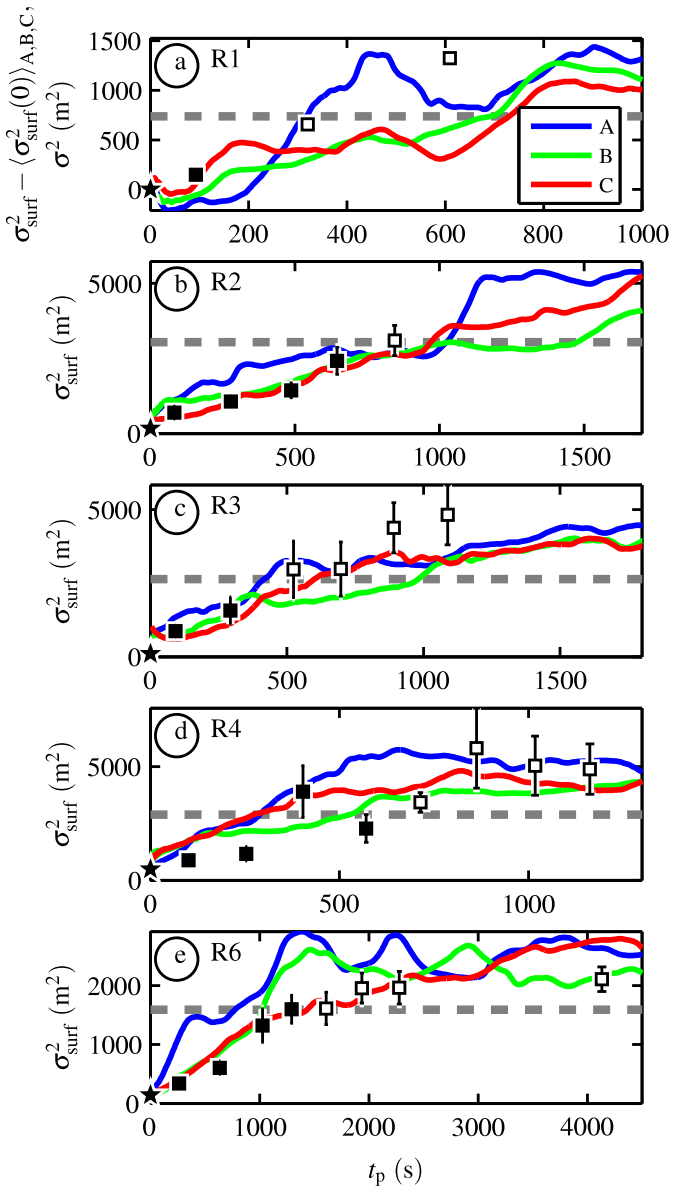

Figure 7. Modeled (color curves) and observed (black or white squares with error bars) squared cross-shore length scale $\sigma^2_{\rm surf}$ versus plume age $t_{\rm p}$ for releases (b) R2, (c) R3, (d) R4, and (e) R6, and (a) $\sigma^{2\,({\rm A,B,C})}_{\rm surf}(t_{\rm p}) - \langle\sigma^{2\,({\rm A,B,C})}_{\rm surf}(t_{\rm p}=0)\rangle_{\rm A,B,C}$ (modeled) and σ^2 (observed) for release R1. Tracer profiles that are well contained in the surfzone, where κ_{xx} is fit, are indicated by black squares (observed) or the region below the dashed gray line (model) with $\mathcal{R} < 0.55$. The $\sigma^{2\,({\rm obs})}_{\rm surf}$ initial conditions (assuming a δ-function at $t_{\rm p} = 0$) are indicated by the black stars. The mean $\sigma^2_{\rm surf}(t_{\rm p})$ skill over releases R2, R3, R4 and R6 is 0.92.

Table 3. Mean model $\langle \kappa_{xx} \rangle_{\mathrm{A,B,C}}$ derived from σ^2_{surf} versus t_{p} (Figure 8).

R1	0.73 ± 0.29
R2	1.02 ± 0.17
R3	1.49 ± 0.30
R4	2.83 ± 0.76
R6	0.67 ± 0.07

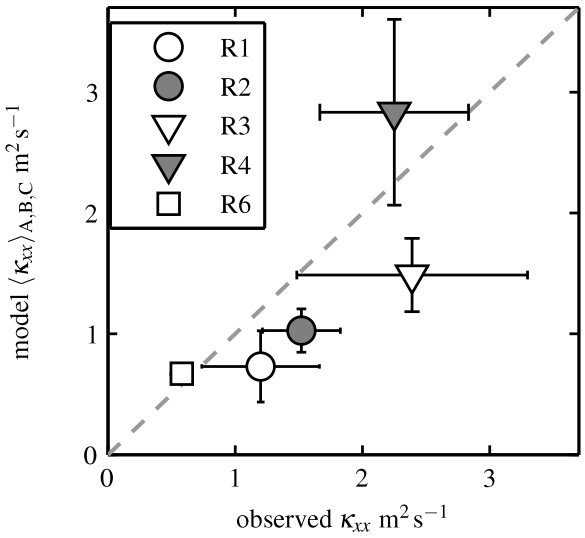

Figure 8. Mean modeled $\langle \kappa_{xx} \rangle_{\mathrm{A,B,C}}$ versus observed $\kappa^{(\mathrm{obs})}_{\mathrm{xx}}$, with a dashed line indicating perfect agreement. The $\kappa^{(\mathrm{obs})}_{\mathrm{xx}}$ and $\langle \kappa_{xx} \rangle_{\mathrm{A,B,C}}$ error bars are estimated from the σ^2_{surf} versus t_{p} fit slope errors as detailed in *Clark et al.* [2010]. The skill is 0.40.

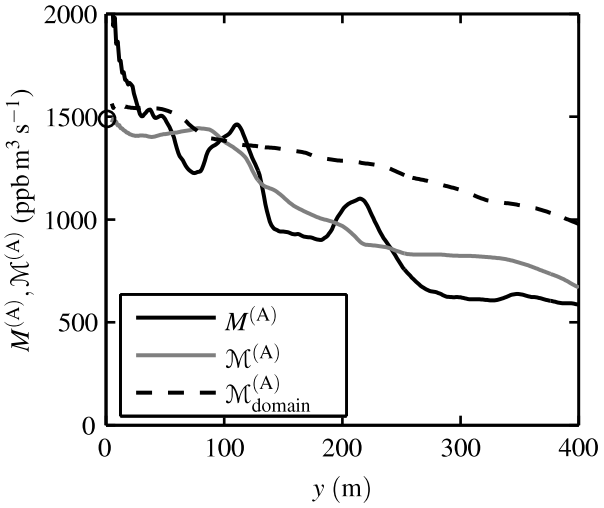

Figure 9. Alongshore tracer transport estimates $M^{(A)}$ (2), $\mathcal{M}^{(A)}$ (7), and $\mathcal{M}^{(A)}_{\rm domain}$ (see legend) versus y for R4. Note that $\mathcal{M}^{(A)}_{\rm domain}$ is defined similar to $\mathcal{M}^{(A)}$, but is integrated over the entire cross-shore tracer domain. Mean and eddy fluxes are included in both $\mathcal{M}^{(A)}$ and $\mathcal{M}^{(A)}_{\rm domain}$. The observed dye release rate is given by the open black circle at $y = 0$ m.

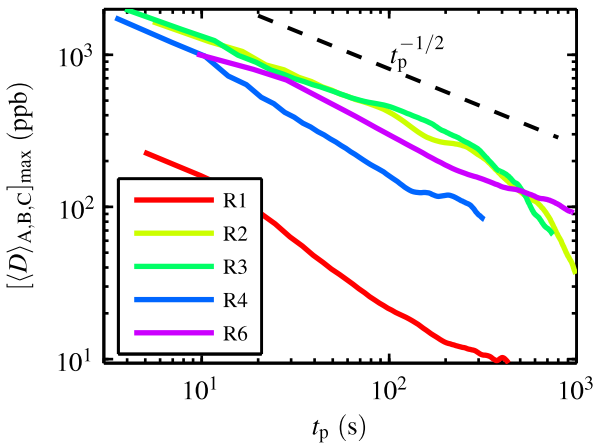

Figure 10. Mean (over tracers A, B, and C) cross-shore tracer maxima $[\langle D \rangle_{\rm A,B,C}]_{\rm max}$ versus plume age $t_{\rm p}$, for the downstream region where tracer is well contained within the surfzone (i.e., the region where κ_{xx} is estimated). The $t_{\rm p}^{-1/2}$ slope based on Fickian diffusion is indicated by the dashed black line.

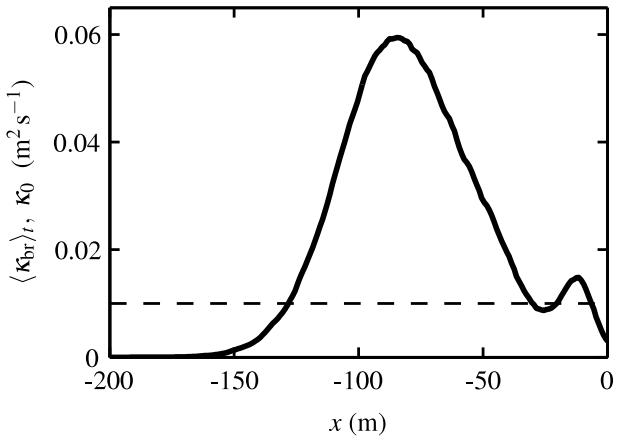

Figure 11. Time-averaged breaking wave diffusivity $\langle \kappa_{\rm br} \rangle_t$ (solid) and background diffusivity $\kappa_0 = 0.01\ {\rm m}^2\,{\rm s}^{-1}$(dashed) versus x for R4.

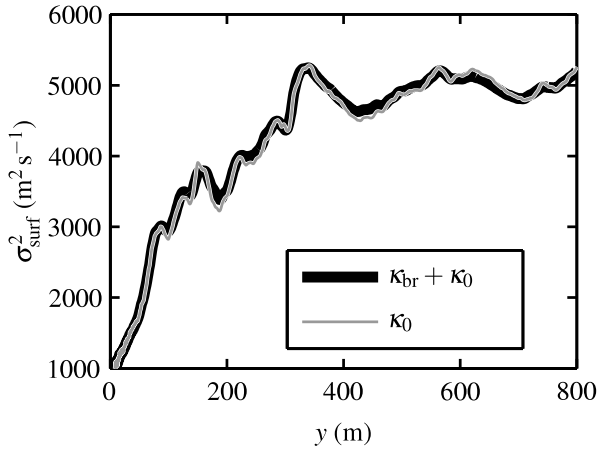

Figure 12. Model $\sigma^2_{\rm surf}$ versus y for two R4 tracers with identical release location: one with full breaking-induced diffusivity $\kappa_{\rm br} + \kappa_0$ (black) and another with background diffusivity κ_0 only (gray).

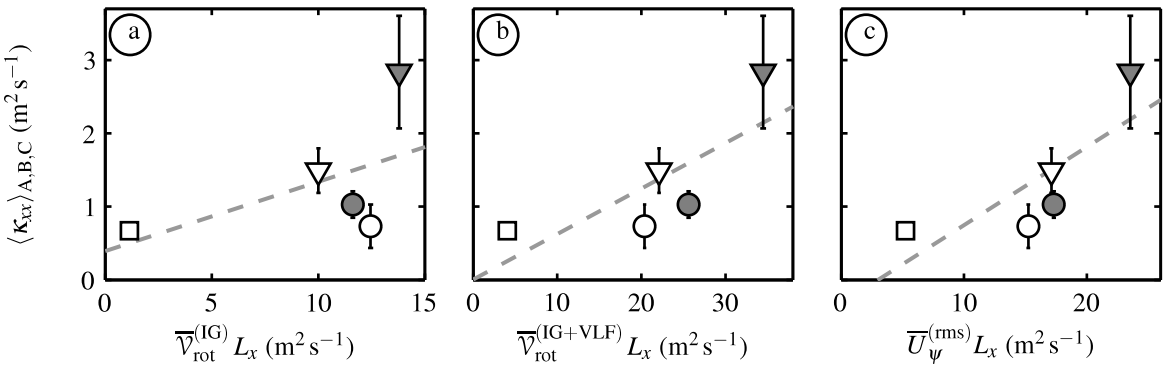

Figure 13. Model $\langle \kappa_{xx} \rangle_{\mathrm{A,B,C}}$ versus (a) $\overline{\mathcal{V}}^{(\mathrm{IG})}_{\mathrm{rot}} L_x$, (b) $\overline{\mathcal{V}}^{(\mathrm{IG+VLF})}_{\mathrm{rot}} L_x$ and (c) $\overline{U}^{(\mathrm{rms})}_{\psi} L_x$ scalings. The dashed gray line indicates linear fits to each scaling, and r^2 correlations are (a) 0.29, (b) 0.60, and (c) 0.63.